



ASTRO-H Space X-ray Observatory White Paper

Stars – Accretion, Shocks, Charge Exchanges and Magnetic Phenomena

Y. Tsuboi (Chuo University), K. Ishibashi (Nagoya University), M. Audard (Université de Genève),
K. Hamaguchi (UMBC/NASA), M. A. Leutenegger (UMBC/NASA), Y. Maeda (JAXA),
K. Mori (Miyazaki University), H. Murakami (Rikkyo University), Y. Sugawara (Chuo University), and
M. Tsujimoto (JAXA)
on behalf of the ASTRO-H Science Working Group

Abstract

X-ray emission from stars has origins as diverse as the stars themselves: accretion shocks, shocks generated in wind-wind collisions, or release of magnetic energy. Although the scenarios responsible for X-ray emission are thought to be known, the physical mechanisms operating are in many cases not yet fully understood. Full testing of many of these mechanisms requires high energy resolution, large effective area, and coverage of broad energy bands. The loss of the X-ray calorimeter spectrometer on board *ASTRO-E2* was a huge blow to the field; it would have provided a large sample of high resolution spectra of stars with high signal-to-noise ratio. Now, with the advent of the *ASTRO-H* Soft X-ray Spectrometer and Hard X-ray Imager, we will be able to examine some of the hot topics in stellar astrophysics and solve outstanding mysteries.

Complete list of the ASTRO-H Science Working Group

Tadayuki Takahashi^a, Kazuhisa Mitsuda^a, Richard Kelley^b, Felix Aharonian^c, Hiroki Akamatsu^d, Fumie Akimoto^e, Steve Allen^f, Naohisa Anabuki^g, Lorella Angelini^b, Keith Arnaud^b, Marc Audardⁱ, Hisamitsu Awaki^j, Aya Bamba^k, Marshall Bautz^l, Roger Blandford^f, Laura Brenneman^b, Greg Brown^m, Edward Cackettⁿ, Maria Chernyakova^c, Meng Chiao^b, Paolo Coppi^o, Elisa Costantini^d, Jelle de Plaa^d, Jan-Willem den Herder^d, Chris Done^p, Tadayasu Dotani^a, Ken Ebisawa^a, Megan Eckart^b, Teruaki Enoto^q, Yuichiro Ezoe^r, Andrew Fabianⁿ, Carlo Ferrignoⁱ, Adam Foster^s, Ryuichi Fujimoto^t, Yasushi Fukazawa^u, Stefan Funk^f, Akihiro Furuzawa^e, Massimiliano Galeazzi^v, Luigi Gallo^w, Poshak Gandhi^p, Matteo Guainazzi^x, Yoshito Haba^y, Kenji Hamaguchi^h, Isamu Hatsukade^z, Takayuki Hayashi^a, Katsuhiro Hayashi^a, Kiyoshi Hayashida^g, Junko Hiraga^{aa}, Ann Hornschemeier^b, Akio Hoshino^{ab}, John Hughes^{ac}, Una Hwang^{ad}, Ryo Iizuka^a, Yoshiyuki Inoue^a, Hajime Inoue^a, Kazunori Ishibashi^e, Manabu Ishida^a, Kumi Ishikawa^q, Yoshitaka Ishisaki^f, Masayuki Ito^{ae}, Naoko Iyomoto^{af}, Jelle Kaastra^d, Timothy Kallman^b, Tuneyoshi Kamae^f, Jun Kataoka^{ag}, Satoru Katsuda^a, Junichiro Katsuta^u, Madoka Kawaharada^a, Nobuyuki Kawai^{ah}, Dmitry Khangulyan^a, Caroline Kilbourne^b, Masashi Kimura^{ai}, Shunji Kitamoto^{ab}, Tetsu Kitayama^{aj}, Takayoshi Kohmura^{ak}, Motohide Kokubun^a, Saori Konami^r, Katsuji Koyama^{al}, Hans Krimm^b, Aya Kubota^{am}, Hideyo Kunieda^e, Stephanie LaMassa^o, Philippe Laurent^{an}, François Lebrun^{an}, Maurice Leutenegger^b, Olivier Limousin^{an}, Michael Loewenstein^b, Knox Long^{ao}, David Lumb^{ap}, Grzegorz Madejski^f, Yoshitomo Maeda^a, Kazuo Makishima^{aa}, Maxim Markevitch^b, Hironori Matsumoto^e, Kyoko Matsushita^{aq}, Dan McCammon^{af}, Brian McNamara^{as}, Jon Miller^{at}, Eric Miller^l, Shin Mineshige^{au}, Ikuyuki Mitsuishi^e, Takuya Miyazawa^e, Tsunefumi Mizuno^u, Koji Mori^z, Hideyuki Mori^e, Koji Mukai^b, Hiroshi Murakami^{av}, Toshio Murakami^t, Richard Mushotzky^h, Ryo Nagino^g, Takao Nakagawa^a, Hiroshi Nakajima^g, Takeshi Nakamori^{aw}, Shinya Nakashima^a, Kazuhiro Nakazawa^{aa}, Masayoshi Nobukawa^{al}, Hirofumi Noda^q, Masaharu Nomachi^{ax}, Steve O' Dell^{ay}, Hirokazu Odaka^a, Takaya Ohashi^r, Masanori Ohno^u, Takashi Okajima^b, Naomi Ota^{az}, Masanobu Ozaki^a, Frits Paerels^{ba}, Stéphane Paltaniⁱ, Arvind Parmar^x, Robert Petre^b, Ciro Pintoⁿ, Martin Pohlⁱ, F. Scott Porter^b, Katja Pottschmidt^b, Brian Ramsey^{ay}, Rubens Reis^{at}, Christopher Reynolds^h, Claudio Ricci^{au}, Helen Russellⁿ, Samar Safi-Harb^{bb}, Shinya Saito^a, Hiroaki Sameshima^a, Goro Sato^{ag}, Kosuke Sato^{aq}, Rie Sato^a, Makoto Sawada^k, Peter Serlemitsos^b, Hiromi Seta^{bc}, Aurora Simionescu^a, Randall Smith^s, Yang Soong^b, Łukasz Stawarz^a, Yasuharu Sugawara^{bd}, Satoshi Sugita^j, Andrew Szymkowiak^o, Hiroyasu Tajima^e, Hiromitsu Takahashi^u, Hiroaki Takahashi^g, Yoh Takei^a, Toru Tamagawa^q, Takayuki Tamura^a, Keisuke Tamura^e, Takaaki Tanaka^{al}, Yasuo Tanaka^a, Yasuyuki Tanaka^u, Makoto Tashiro^{bc}, Yuzuru Tawara^e, Yukikatsu Terada^{bc}, Yuichi Terashima^j, Francesco Tombesi^b, Hiroshi Tomida^{ai}, Yohko Tsuboi^{bd}, Masahiro Tsujimoto^a, Hiroshi Tsunemi^g, Takeshi Tsuru^{al}, Hiroyuki Uchida^{al}, Yasunobu Uchiyama^{ab}, Hideki Uchiyama^{be}, Yoshihiro Ueda^{au}, Shutaro Ueda^g, Shiro Ueno^{ai}, Shinichiro Uno^{bf}, Meg Urry^o, Eugenio Ursino^v, Cor de Vries^d, Shin Watanabe^a, Norbert Werner^f, Dan Wilkins^w, Shinya Yamada^r, Hiroya Yamaguchi^b, Kazutaka Yamaoka^e, Noriko Yamasaki^a, Makoto Yamauchi^z, Shigeo Yamauchi^{az}, Tahir Yaqoob^b, Yoichi Yatsu^{ah}, Daisuke Yonetoku^t, Atsumasa Yoshida^k, Takayuki Yuasa^q, Irina Zhuravleva^f, Abderahmen Zoghbi^h, and John ZuHone^b

^aInstitute of Space and Astronautical Science (ISAS), Japan Aerospace Exploration Agency (JAXA), Kanagawa 252-5210, Japan

^bNASA/Goddard Space Flight Center, MD 20771, USA

^cAstronomy and Astrophysics Section, Dublin Institute for Advanced Studies, Dublin 2, Ireland

^dSRON Netherlands Institute for Space Research, Utrecht, The Netherlands

^eDepartment of Physics, Nagoya University, Aichi 338-8570, Japan

^fKavli Institute for Particle Astrophysics and Cosmology, Stanford University, CA 94305, USA

^gDepartment of Earth and Space Science, Osaka University, Osaka 560-0043, Japan

^hDepartment of Astronomy, University of Maryland, MD 20742, USA

ⁱUniversité de Genève, Genève 4, Switzerland

^jDepartment of Physics, Ehime University, Ehime 790-8577, Japan

^kDepartment of Physics and Mathematics, Aoyama Gakuin University, Kanagawa 229-8558, Japan

^lKavli Institute for Astrophysics and Space Research, Massachusetts Institute of Technology, MA 02139, USA

^mLawrence Livermore National Laboratory, CA 94550, USA

ⁿInstitute of Astronomy, Cambridge University, CB3 0HA, UK

^oYale Center for Astronomy and Astrophysics, Yale University, CT 06520-8121, USA

^pDepartment of Physics, University of Durham, DH1 3LE, UK

^qRIKEN, Saitama 351-0198, Japan

^rDepartment of Physics, Tokyo Metropolitan University, Tokyo 192-0397, Japan

^sHarvard-Smithsonian Center for Astrophysics, MA 02138, USA

- ^tFaculty of Mathematics and Physics, Kanazawa University, Ishikawa 920-1192, Japan
- ^uDepartment of Physical Science, Hiroshima University, Hiroshima 739-8526, Japan
- ^vPhysics Department, University of Miami, FL 33124, USA
- ^wDepartment of Astronomy and Physics, Saint Mary's University, Nova Scotia B3H 3C3, Canada
- ^xEuropean Space Agency (ESA), European Space Astronomy Centre (ESAC), Madrid, Spain
- ^yDepartment of Physics and Astronomy, Aichi University of Education, Aichi 448-8543, Japan
- ^zDepartment of Applied Physics, University of Miyazaki, Miyazaki 889-2192, Japan
- ^{aa}Department of Physics, University of Tokyo, Tokyo 113-0033, Japan
- ^{ab}Department of Physics, Rikkyo University, Tokyo 171-8501, Japan
- ^{ac}Department of Physics and Astronomy, Rutgers University, NJ 08854-8019, USA
- ^{ad}Department of Physics and Astronomy, Johns Hopkins University, MD 21218, USA
- ^{ae}Faculty of Human Development, Kobe University, Hyogo 657-8501, Japan
- ^{af}Kyushu University, Fukuoka 819-0395, Japan
- ^{ag}Research Institute for Science and Engineering, Waseda University, Tokyo 169-8555, Japan
- ^{ah}Department of Physics, Tokyo Institute of Technology, Tokyo 152-8551, Japan
- ^{ai}Tsukuba Space Center (TKSC), Japan Aerospace Exploration Agency (JAXA), Ibaraki 305-8505, Japan
- ^{aj}Department of Physics, Toho University, Chiba 274-8510, Japan
- ^{ak}Department of Physics, Tokyo University of Science, Chiba 278-8510, Japan
- ^{al}Department of Physics, Kyoto University, Kyoto 606-8502, Japan
- ^{am}Department of Electronic Information Systems, Shibaura Institute of Technology, Saitama 337-8570, Japan
- ^{an}IRFU/Service d'Astrophysique, CEA Saclay, 91191 Gif-sur-Yvette Cedex, France
- ^{ao}Space Telescope Science Institute, MD 21218, USA
- ^{ap}European Space Agency (ESA), European Space Research and Technology Centre (ESTEC), 2200 AG Noordwijk, The Netherlands
- ^{aq}Department of Physics, Tokyo University of Science, Tokyo 162-8601, Japan
- ^{ar}Department of Physics, University of Wisconsin, WI 53706, USA
- ^{as}University of Waterloo, Ontario N2L 3G1, Canada
- ^{at}Department of Astronomy, University of Michigan, MI 48109, USA
- ^{au}Department of Astronomy, Kyoto University, Kyoto 606-8502, Japan
- ^{av}Department of Information Science, Faculty of Liberal Arts, Tohoku Gakuin University, Miyagi 981-3193, Japan
- ^{aw}Department of Physics, Faculty of Science, Yamagata University, Yamagata 990-8560, Japan
- ^{ax}Laboratory of Nuclear Studies, Osaka University, Osaka 560-0043, Japan
- ^{ay}NASA/Marshall Space Flight Center, AL 35812, USA
- ^{az}Department of Physics, Faculty of Science, Nara Women's University, Nara 630-8506, Japan
- ^{ba}Department of Astronomy, Columbia University, NY 10027, USA
- ^{bb}Department of Physics and Astronomy, University of Manitoba, MB R3T 2N2, Canada
- ^{bc}Department of Physics, Saitama University, Saitama 338-8570, Japan
- ^{bd}Department of Physics, Chuo University, Tokyo 112-8551, Japan
- ^{be}Science Education, Faculty of Education, Shizuoka University, Shizuoka 422-8529, Japan
- ^{bf}Faculty of Social and Information Sciences, Nihon Fukushi University, Aichi 475-0012, Japan

Contents

1	X-ray Stellar Astrophysics	5
2	Protostars	6
2.1	Background and Previous Studies	6
2.2	Prospects & Strategy	6
2.3	Targets & Feasibility	8
3	Flare Physics in Low-mass Stars	10
3.1	Background and Previous Studies	10
3.2	Prospects & Strategy	10
3.2.1	Dynamic movement of materials during Flares	10
3.2.2	Particle Acceleration in Flares	11
3.2.3	Star-Planet Interaction	11
3.3	Targets & Feasibility	13
3.3.1	Flare Stars	13
3.3.2	Planet-hosting Stars	13
4	Accretion Processes in Classical T Tauri Stars	15
4.1	Background and Previous Studies	15
4.2	Prospects & Strategy	16
4.3	Targets & Feasibility	17
4.4	Beyond Feasibility	18
5	Colliding Winds in Massive Stars	19
5.1	Background and Previous Studies	19
5.2	Prospects & Strategy	19
5.2.1	Broad-band spectroscopy	19
5.2.2	Spectral lines	20
5.3	Targets & Feasibility	20
5.4	Beyond Feasibility	21
6	Diffuse X-rays Associated with Star Forming Regions	23
6.1	Background and Previous Studies	23
6.2	Prospects & Strategy	23
6.3	Targets & Feasibility	24

1 X-ray Stellar Astrophysics

For understanding the universe and its evolution it is imperative to understand the physics of stellar phenomena, as stars are one of the most fundamental constituents of the universe. Stars have a major influence on the dynamical state of surrounding media and enriches them chemically with a fresh injection of heavy metals through their slow or rapid evolution. Stars eventually evolve into other exotic objects, such as white dwarfs, neutron stars, or a black hole. In the process, stars may explode, as in supernova explosions.

But what happens if our understanding of stars is not adequate?

The physical models and mechanisms describing exotic objects are based on the best knowledge of stellar physics. If the foundation of our understanding for stars stands on shaky ground, then astrophysics – and cosmology – may be in peril.

And we understand them very little: how does a flare occur in stars? Even magnetic activity on the Sun is not fully understood. How does coronal heating occur in non-solar-type objects (or is it identical)? What is the accretion geometry in very young stars? What density does a pre-natal cocoon of a young star typically have?

In this section, we focus on three key aspects of the *ASTRO-H* mission: high energy resolution (5 – 7 eV), highly accurate energy determination (i.e., stable gain) of Soft X-ray Spectrometer (SXS) and its broad-band capability combined with Soft and Hard X-ray Imagers (SXI and HXI).

For instance on flaring stars, the SXS provides sufficient energy resolution to construct reliable differential emission measure at the high-temperature end using Fe and Ni K emission lines; at the same time, the HXI will allow the same flare to be probed at energies greater than 10 keV and finally to place a constraint on the low cut-off energy in accelerated electrons, fully accounting the amount of energy released by a flaring mechanism (hence leading to better understanding of the mechanism itself).

Much like flaring stars, interactions of massive stars' winds can be probed as well with the combination of SXI + SXS + HXI to reveal the physical state of stellar wind shocks. Furthermore, for the first time, *ASTRO-H* may be able to detect inverse Compton emission in its hard X-ray tail and to reveal its connection with known thermal radiation seen in them.

A traditional method of line diagnostics is valid as well for studies in classical T-Tauri stars. At a higher energy ($E \geq 1$ keV), the advantage exists in the SXS to probe local densities (10^{11} to 10^{13} cm⁻³) associated with regions in which the emission of Ne IX and Mg XI triplets emerge. This will enable us to probe X-ray emission of young stars for which accretion plays a major role.

For studies of protostars and diffuse X-ray emission surrounding star formation region, the two key aspects of the SXS become crucial: high energy resolution and highly accurate energy determination for dynamic studies. A rotating core of a protostar is so deeply embedded in its prenatal cocoon and cannot be probed directly. But the shape and centroid position of He-like and fluorescent Fe line tells the story about its origin in an accreting disk. A dynamic-broadening signature, expected from an accreting disk around a protostar, is in order of 300 km s⁻¹, typically. With the energy resolution of 5 eV and the energy determination accuracy of 0.5 eV, the detection of such a Doppler signature is well within the realm of possibility. For diffused X-ray emission, the same skill can be applied to separate unidentified emission lines observed in CCD spectra from known thermal emission lines as well, as their identification requires measurements of their line center energies at less than a few eV uncertainty.

Astrophysicists have models to ascribe X-ray phenomena witnessed in those stellar targets, but not enough data to test them with rigor. So we have awaited the advent of the Soft X-ray Spectrometer on board *ASTRO-H*. In conjunction with other instruments, especially the Hard X-ray Imagers, we will be able to explore a new horizon to extend our understanding of stars and related phenomena.

2 Protostars

2.1 Background and Previous Studies

Low-mass young stellar objects (YSOs) evolve from molecular cloud cores through the protostar, Classical T Tauri (CTTS) and Weak-line T Tauri (WTTS) phases to the main sequence. Protostars are generally associated with Class 0 and I spectra, with spectral energy distributions (SEDs) which peak in the mm and mid- to far-IR bands, respectively. Bipolar flows accompany this phase, indicating dynamic gas accretion. However, due to very high extinction in the optical band, the vicinity of the *protostar itself* and the process of accretion onto the central star had never been directly observed.

This breakthrough was achieved in *hard* X-rays due to high transparency of the ISM in this band. X-rays from protostars were discovered with *ASCA* in ρ Oph (Koyama et al., 1994) and detailed analyses were performed by Kamata et al. (1997). They detected three Class I protostars, which all have a spectrum characterized by heavy absorption ($N_{\text{H}} > 10^{22} \text{ cm}^{-2}$) and highly ionized iron K shell lines. The spectra are well-fitted with optically thin thermal plasma model with $kT > 1 \text{ keV}$. Who would have expected that the central star in a molecular core has such high temperature gas, while the molecular core has only tens of Kelvin? Flare-like time variability was observed in one of the Class I protostars (EL 29). Such variability is seen on the solar surface and implies magnetic activity on/near the central star of the protostar. The time scale of the flare and the temperature of the gas are greater than those in solar flares, and the X-ray luminosity of the protostar is 10^3 – 10^6 times greater than solar flares.

The Class I protostar WL 6 showed a sinusoidal light curve with a period of about one day, and with constant temperature, which suggests rotational modulation of the protostar (Kamata et al., 1997). On the other hand, the Class I protostar YLW 15A showed quasi-periodic X-ray flares with about 20 hour intervals (Tsuboi et al., 2000). The flares can be interpreted as a star-disk interaction in which the star itself is rotating rapidly with 1 day spin period (Montmerle et al., 2000). The period of 1 day is significantly shorter than the spin periods in the other phases (about 7 days in Class II and 3 days in Class III). If the stellar spin is truly 1 day, the central star might rotate with nearly break-up velocity. The rotation period is undoubtedly a key parameter for accretion onto protostars; it is a direct indicator for the accumulated angular momentum of the star itself. These results have demonstrated that we can derive the fundamental parameter uniquely with hard X-ray band.

It was demonstrated that we can probe not only the protostar itself, but also its close vicinity, using emission lines. Imanishi et al. (2001) discovered a fluorescent iron line at 6.4 keV as well as the highly ionized iron line at 6.7 keV from one of the protostars, YLW16A, in its flare phase. Similar spectra have been observed in type I Seyfert galaxies. Based on this similarity, they interpret that the incident X-rays emitted from the protostar itself irradiate a surrounding cold material which then re-emits fluorescent lines. The large equivalent width (100 eV) and not so large absorption column ($5 \times 10^{22} \text{ cm}^{-2}$) is comparable to what is observed in type I Seyfert galaxies. If the circumstellar gas is spherically distributed around the X-ray source, the equivalent width of the iron line is predicted to be just $\sim 15 \text{ eV}$. Hence, nonspherical geometry is required; a larger amount of gas is present out of the line of sight, i.e. reflection by a face-on disk is plausible (Sekimoto et al., 1997). Since the time lag between the flare onset and the 6.4 keV iron line appearance is shorter than 3 hours, the separation between the star and the reflecting region is $\leq 20 \text{ AU}$, consistent with a disk origin. After this discovery, neutral Fe fluorescent lines were also detected from other several embedded sources (Tsujiimoto et al. 2004, Hamaguchi et al. 2005), including our proposed target R CrA IRS 7.

2.2 Prospects & Strategy

With the above insights, we believe that we can probe the structure and the dynamics of central stars in dense molecular cores and those of the vicinities using the following methods. Although observations of radio masars can probe in to a distance of about 10 AU from the central protostar, the most inner part can only be revealed with the high-resolution spectroscopic capability of the SXS.

(1) The spin and the radius of the central star of a protostar

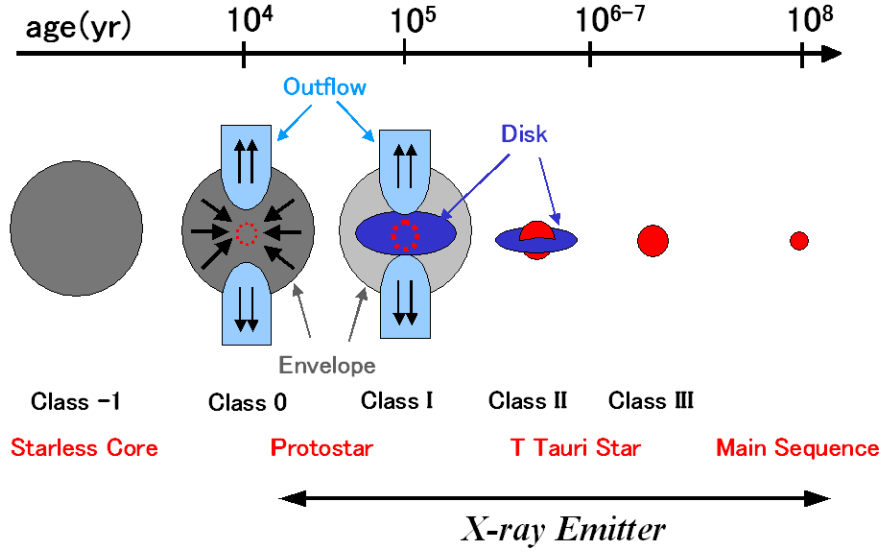


Figure 1: Schematic view of star formation. Protostars are classified as Class 0 and I, which have SED peaks in the *mm* and mid- to far-IR bands, respectively. Bipolar flows accompany these phases, indicating dynamic gas accretion.

By monitoring the doppler-shifted He-like iron line (6.7 keV), we will obtain a rotation period of the X-ray-active region possibly on the protostar itself, directly. If a protostar has a radius of $\sim 5R_{\odot}$ and a rotation period of 1 day, the maximum Doppler velocity broadening due to this rotation are $\sim 350 \text{ km s}^{-1} \sin i$ and $8 \text{ eV} \sin i$ at 7 keV, respectively, where i is the inclination angle of the star's rotational axis. The *ASTRO-H* SXS, with its superior spectral resolution ($E/\Delta E = 1000$) at 7 keV, is the only spectrometer capable of detecting this Doppler broadening. This measurement can be used to infer the stellar radius:

$$2\pi R_* \cos \theta \sin i = v \cos \theta \sin i T, \quad (1)$$

where θ is the latitude of the active region and i is the inclination angle of the stellar rotation axis. The spin velocity and the stellar radius probe the angular momentum of the protostar itself, which is crucial in understanding the contraction process of a star.

(2) The dynamics of the accreting matter

The accretion disk of a protostar emits 6.4 keV photons from neutral iron due to fluorescence by hard X-rays from the star itself. By measuring the Doppler shift and broadening of this line we will characterize the dynamics of the inner part of the disk. The differences of orbital period and velocity between the disk and the stellar surface, as characterized by the 6.7 keV, allow us to understand the transfer of angular momentum from the disk to the star.

As with the 6.7 keV line, we can derive the radius of the 6.4 keV emitting region. In this case, by assuming Keplerian motion, we can also obtain a lower limit to the enclosed mass, i.e. the mass of the protostar itself.

By making time-sliced spectra during a flare and measuring the neutral Fe K equivalent width, as Imanishi et al. (2001) did, we can construct a map of the structure of the inner accretion disk. Because of the high sensitivity of the SXS in the Fe K band in comparison with *Chandra*, we can characterize this structure with higher resolution. The structure of the inner part of the protostellar accretion disks is of particular interest, since these disks will evolve into planetary disks.

(3) Acceleration of the jets from protostars

Pravdo et al. (2001) detected jets from the protostar HH2 for the first time in the X-ray band. The velocity of the bulk motion of the jets was estimated as 200 km s^{-1} from the plasma temperature. Favata et al. (2002), Bally et al. (2003), Tsujimoto et al. (2004), and other recent studies also found fast X-ray jets with a speed of $500\text{--}1000 \text{ km s}^{-1}$. Jets are expected to accompany X-ray flares, which occur due to magnetic reconnection events (e.g., Hayashi et al. 1996). In fact, such phenomena have been observed on the Solar surface. The *ASTRO-H* SXS can search for co-existence of X-ray flares and jets from a protostar by looking for the Doppler signature of the jet in emission lines contemporaneously with an increase in count rate.

(4) Plasma temperature

In past protostar surveys, it has been found that younger stars have X-ray emission from higher temperature plasma. However, in significant numbers of protostars, the temperatures are not well-determined, owing to limited statistics, heavy circumstellar absorption, and the drop in sensitivity of conventional X-ray telescopes above 10 keV. Measurements of the line ratios between He-like Fe at 6.7 keV and the H-like Fe at 6.9 keV allow us to infer plasma temperatures independently of the X-ray continuum spectrum. The sensitivity of SXS in the Fe K band will allow us to determine the temperature with unparalleled precision.

(5) The turn-on age of stellar X-rays

ASCA detected X-rays from embedded Class I protostars (Koyama et al., 1994) and *Chandra* is now establishing the X-ray properties of Class I. Seventy percent of Class I objects were detected in a 100 ks *Chandra* observation of the Ophiuchi cloud (Imanishi et al., 2001), demonstrating that virtually all Class I YSOs emit X-rays. On the other hand, none of the 41 pre-stellar Class 0 cores in the Ophiuchi cloud were detected (Figure 1), indicating that the protostar itself is essential for X-ray production. These results indicate that X-rays turn on at some point during the Class 0 phase, but the precise turn-on age is still an open question.

Some Class 0 protostars have been tentatively detected as X-ray sources, but whether these sources are bona-fide Class 0 objects is still controversial: in the $\text{Log } M_{\text{env}} - \text{Log } L_{\text{bol}}$ diagram, they are all located in the region corresponding to the Class I phase or the boundary region between the Class I and 0 phases (Getman et al., 2007). The difficulty in detecting X-ray emission from bona-fide Class 0 protostars might be due to the presence of larger absorbing columns than those in Class I protostars. The hard X-ray band above 10 keV is even more transparent than the *Chandra* band, and thus the *ASTRO-H* HXI is extremely sensitive to X-rays from protostars embedded in thick clouds of with circumstellar absorbing columns of $N_H \geq 10^{24} \text{ cm}^{-2}$.

(6) Probing of soft gamma-ray precursor of flares

Solar flares show a precursor to thermal X-ray flares in the non-thermal soft gamma-ray band (e.g., Sakao et al., 1992). The precursor is thought to be non-thermal bremsstrahlung emission which occurs as a result of particle acceleration during magnetic reconnection events. No apparent precursor has yet been observed from stars other than the Sun. The HXI will be very sensitive to this precursor emission, while the SXI and SXS will detect K-shell lines from highly ionized Fe emitted in the thermal part of flares. The combination of these *ASTRO-H* instruments is a strong tool in characterizing the flaring process in protostars.

2.3 Targets & Feasibility

There are two nearby young stellar clusters that include protostars bright enough to do spectroscopy with the *ASTRO-H* SXS calorimeter: ρ Oph ($d \sim 165 \text{ pc}$), and R CrA ($d \sim 130 \text{ pc}$). In the $2.9' \times 2.9'$ field of view of the SXS, four Class I protostars can be included in an observation of part of the ρ Oph region, and three Class I protostars and two Class 0 protostars can be included in an observation of the R CrA region.

To verify the rotational period of a given system to be ~ 1 day, we should compare the X-ray spectra of each 20 ksec ($\sim 1/4$ day). The observing efficiency of *ASTRO-H* will allow us to achieve 10 ksec effective exposure. Assuming $L = 10^{31} \text{ ergs s}^{-1}$, $kT = 6 \text{ keV}$, $N_H = 3 \times 10^{22} \text{ cm}^{-2}$, and elemental abundances of 0.3 solar, we will be able to constrain the Doppler shift of He-like iron lines with a $1\text{-}\sigma$ uncertainty of 1.5 eV. Thus, the rotational

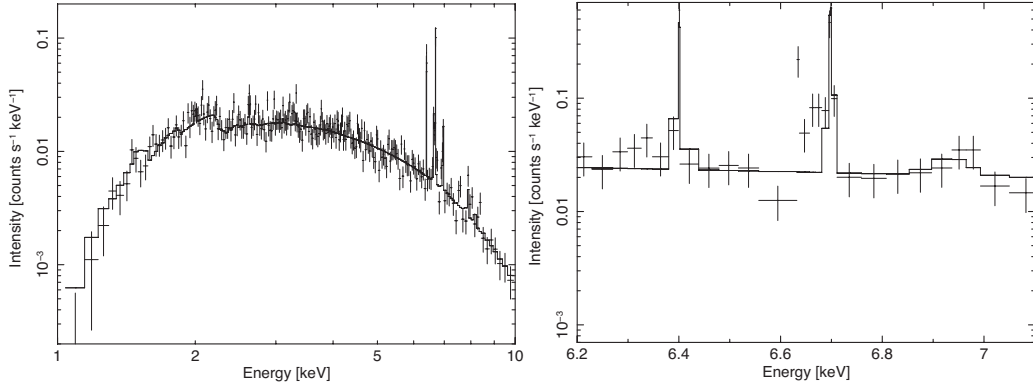


Figure 2: Simulation of the *ASTRO-H/SXS* spectrum of a protostar. Left panel: View of the broadband spectrum, assuming an X-ray luminosity of 1×10^{31} ergs s^{-1} and exposure time of 80 ks. Right: detailed view of the iron K_{α} band. An X-ray luminosity of 4×10^{31} ergs s^{-1} and 10 ks exposure time are assumed ($\sim 1/4$ day with 50% observing efficiency).

speed of the protostar can be determined with 100 km s^{-1} precision. If we detect the 6.4-keV neutral iron line with an equivalent width of 100 eV, the uncertainty on the Doppler shift and broadening will be comparable to that for the 6.7-keV line.

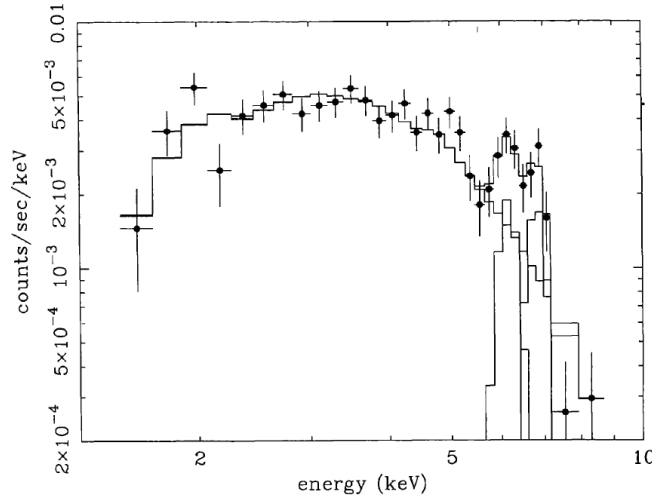


Figure 3: Spectrum observed in a flare of IRS7, obtained with *ASCA* (Koyama et al., 1996).

Note that one of the Class 0 candidates (X_E , or Source 8 in Feigelson et al. 1998) flared during an *XMM-Newton* observation in March 2003 (Hamaguchi et al., 2005). During the flare, a strong Fe K fluorescent line at 6.4 keV was detected with an equivalent width of about 800 eV. Also note that in the *ASCA* observation of this region (Koyama et al., 1996), striking results were obtained: during a flare on IRS 7, two line features appeared with central energy of 6.81 keV and 6.12 keV (Figure 3). If we assume that the 6.12 keV feature is a Doppler-shifted 6.4 keV fluorescent line from neutral iron, the inferred infall speed of the cold material would exceed 10^4 km s^{-1} , which is orders of magnitude larger than expected for low-mass stars. If we catch such an enigmatic flare with the SXS, spectra with clearly resolved lines will be obtained, and the dynamics of the high-speed plasma will be easily resolved.

3 Flare Physics in Low-mass Stars

3.1 Background and Previous Studies

Since the *Chandra* and *XMM-Newton* observatories opened an era of X-ray high-resolution spectroscopy a decade ago, low-mass stars are among the most observed classes of sources by their grating instruments. This is quite reasonable considering that they exhibit diagnostically rich line-dominated spectra and are observationally easy targets. Low-mass stars are active in the X-ray band and hundreds of objects can be found in our proximity which have well-determined stellar parameters and distances, and intense X-ray flux sufficient for high-resolution spectroscopy. They are distributed in Galactic longitude and latitude, thus are visible even when other Galactic targets are not.

The X-ray emission from low-mass stars have been interpreted by extrapolating from the Sun, in which the combination of differential rotation and convection gives rise to surface magnetic fields, with stored energy released in magnetic reconnection events, resulting in the production of high-temperature plasma. However, not all low-mass stars operate identically to the Sun. The Sun is a single star, whereas most X-ray active low-mass stars are binaries. The Sun has a rotation period of ~ 30 days, while other low-mass stars rotate much more rapidly, e.g. BO Mic, with a rotation period of 0.4 days. The Sun hosts a planet system with two gas giants (Jupiter and Saturn) far away from itself, but an increasing number of stars are now known to host gas giants very close to the primary star. All these differences make X-ray emission from low-mass stars different from those of the Sun both quantitatively and qualitatively.

A typical X-ray spectrum obtained in an observation of a low-mass star is a mixture of soft, stable coronal emission, together with occasional hard and transient flare emission. The flares are caused by magnetic reconnection events, while the corona is an integrated energy reservoir. While both *XMM-Newton* and *Chandra* were well-suited to study the former, *ASTRO-H* is best suited for the latter. Although HETG has sensitivity at >2 keV, the effective area is so small that it has not been possible to extract meaningful constraints from Fe K line profiles during stellar flares. Although HXI will have sensitivity similar to *NuSTAR*, simultaneous observation by a high-resolution soft X-ray spectrometer in the soft-band and a sensitive hard-band detector, which is a requisite in flare observations, will only be possible with *ASTRO-H*. It is expected that *ASTRO-H* will yield fruitful results in stellar flare physics, and we discuss selected topics in this field below.

3.2 Prospects & Strategy

3.2.1 Dynamic movement of materials during Flares

Recent solar X-ray observations have revealed dynamic motion during flares. The energy released in magnetic reconnection events is given to charged particles. While upward-moving particles give rise to a coronal mass ejection, downward-moving particles evaporate cold material in the chromosphere, which is trapped as hot plasma in flare loops. Such movements are routinely captured in spatially resolved movies. The movement of coronal material is traced e.g. by Doppler-shifted Fe XV emission (Asai et al., 2008).

Although we cannot obtain spatially resolved observations of stellar flares, there are hints in the integrated spectrum which suggest that such phenomena take place on a much larger scale. For example, Algol is a typical X-ray emitting stellar system, which is comprised of an X-ray dim B star and an X-ray active K star. This source exhibits such frequent X-ray flares that almost all pointed X-ray observations captured a flare (Favata & Schmitt, 1999; Yank et al., 2009).

During a Beppo-SAX observation (Favata & Schmitt, 1999) of Algol, two interesting features were found. First, the elemental abundances inferred from the X-ray spectrum obtained during a flare changed compared to the pre-flare spectrum, and in particular the Fe abundance increased by a factor of a few. This is interpreted as evaporation of Fe in the chromosphere into the corona. Second, photoelectric absorption of the X-ray emitting region increased during the flare, which is interpreted as absorption through coronal mass ejection (CME) material ejected by the flare. These interpretations need to be tested with direct measurements of the motion of the X-ray emitting material. The expected Doppler velocity of ~ 200 km s⁻¹ will be easily distinguished by the

SXS.

3.2.2 Particle Acceleration in Flares

The RHESSI observatory has made revolutionary progress in understanding high-energy phenomena in flares. We expect that *ASTRO-H* will make similar progress in understanding stellar flares in the 10–50 keV band. Figure 4 shows an X4.8 class solar flare observed by the RHESSI observatory (Lin, 2011). The emission is comprised of a thermal component below 30 keV, non-thermal components from 30–1000 keV and nuclear γ -rays above 1 MeV.

The sudden release of magnetic energy in a flare gives rise to accelerated charged particles. Downward-moving particles collide with dense material in the atmosphere, where they emit non-thermal bremsstrahlung as well as nuclear γ -rays. The released energy is thermalized and the flare loop filled with thermal plasma.

The detection of nuclear γ -ray emission from stars is still far below the sensitivity of contemporary technology, but the non-thermal emission is within reach. Osten et al. (2007) reported detection with the *Swift* BAT of hard X-ray emission extending to 200 keV during a giant flare from II Peg. The spectrum was statistically inconclusive as to whether it is due to non-thermal or high-temperature thermal plasma, but it certainly illustrated that >10 keV emission does exist in stellar flares like the Sun.

We expect that *ASTRO-H* will make two major advances in this field. First, it will detect >10 keV X-rays from a number of low-mass stars, greatly expanding the sample over UV Ceti, the only one known to date. In Figure 4, we show the spectrum of a Solar X4.8 class flare, with the righthand y-axis scaled to the luminosity observed by MAXI from a giant flare on UV Cet (Negoro et al., 2012), and with a comparison to the expected sensitivity by the *ASTRO-H* instruments as well as *Suzaku* HXD. The flux of the non-thermal emission is just below the HXD sensitivity but far above that HXI sensitivity, demonstrating that we are standing just at the edge of this discovery space.

ASTRO-H will also conclusively determine whether the >10 keV emission in stellar flares is non-thermal, and will measure the low-energy cutoff the accelerated particles for the brightest cases. The low-energy cut-off is a key parameter which remains to be constrained even in solar flares. The photon index of the non-thermal emission is large (3–6; see Fig 4), so the estimate of the number of accelerated electrons (the electric current from the corona to the photosphere) can vary significantly with a slight change in the low-energy cutoff. If the cutoff energy is 20 keV in a typical solar flare spectrum, the number of accelerated electrons is absurdly large; all the electrons in a volume larger than a solar active region need to be accelerated, resulting in a current of $\approx 10^{18}$ A. There is thus speculation that the cut-off energy in the non-thermal emission is significantly higher than this.

In order to make these measurements, we need to have a combination of (i) a < 10 keV spectrometer with sufficient energy resolution to construct the differential emission measure precisely at the high-temperature end using the Fe and Ni K emission lines and (ii) a sensitive >10 keV detector, with both detectors operating simultaneously to observe the same flare. This combination has never been employed even in solar observations.

3.2.3 Star-Planet Interaction

Since it has become increasingly clear that close-in giant planets are not so uncommon, an enhancement of flaring activity on the host star due to star-planet interactions (SPIs) has been a matter of lively debate (Cuntz et al., 2000; Rubenstein & Schaefer, 2000). SPIs are expected to include not only tidal interactions one but also magnetic interactions that might increase coronal activities and thus could be investigated through X-rays (e.g., Lanza, 2009). If this is the case, an X-ray study of such flare events would be a useful probe of magnetic field strengths and configurations of extra-solar giant planet systems. Although X-ray investigations of individual systems and statistical samples have been both carried out (Miller et al., 2012, and references therein), the results have been mixed, and high-energy activity induced by SPIs is still controversial. High quality data to derive more reliable physical parameters, such as plasma density and temperature, are in strong demand.

Since the time duration of X-ray flares observed so far from giant planet systems is typically short (~ 10 ks in the case of HD 189733; Pillitteri et al. 2010, 2011) the large effective area and high energy resolution provided

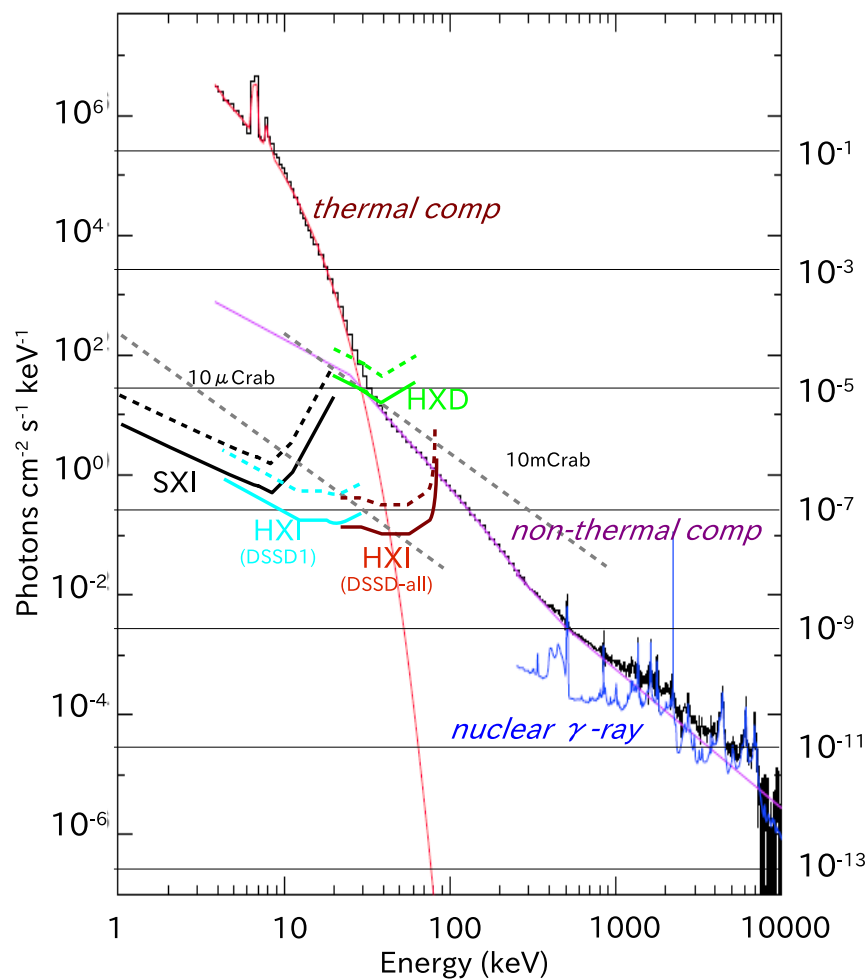


Figure 4: Spectrum of an X4.8 class Solar flare (Lin, 2011), with the righthand y-axis scaled to the luminosity of a giant stellar flare observed in UV Cet (Negoro et al., 2012). The flare consists of three major spectral components (thermal, non-thermal, nuclear γ -ray lines). The SXI, HXI, and *Suzaku*/HXD sensitivity for 100 ks observations (and for 1/10 flux) is shown with solid (dashed) curves.

by the SXS are required to determine the plasma density and temperature of the flares. The SXS has four times more effective area than the *XMM-Newton* and *Chandra* gratings near 1 keV in the Ne K band, which is especially useful to constrain the coronal density of the host star that, which in the case of HD 189733 has been suggested to be unusually dense (Pillitteri et al., 2011).

3.3 Targets & Feasibility

3.3.1 Flare Stars

Sufficiently bright sources are needed to make use of the high-resolution spectroscopic capability of the SXS, which has 2^{14} spectral bins. In order to have a few counts per bin within a reasonable exposure time, we require sources with brightness of at least a few mCrab on average. Fortunately, we have hundreds of sources (Makarov, 2003) to choose from. Some of these sources exhibit flares so frequently that it is almost certain that we will detect a flare or two in a ≈ 100 ks exposure.

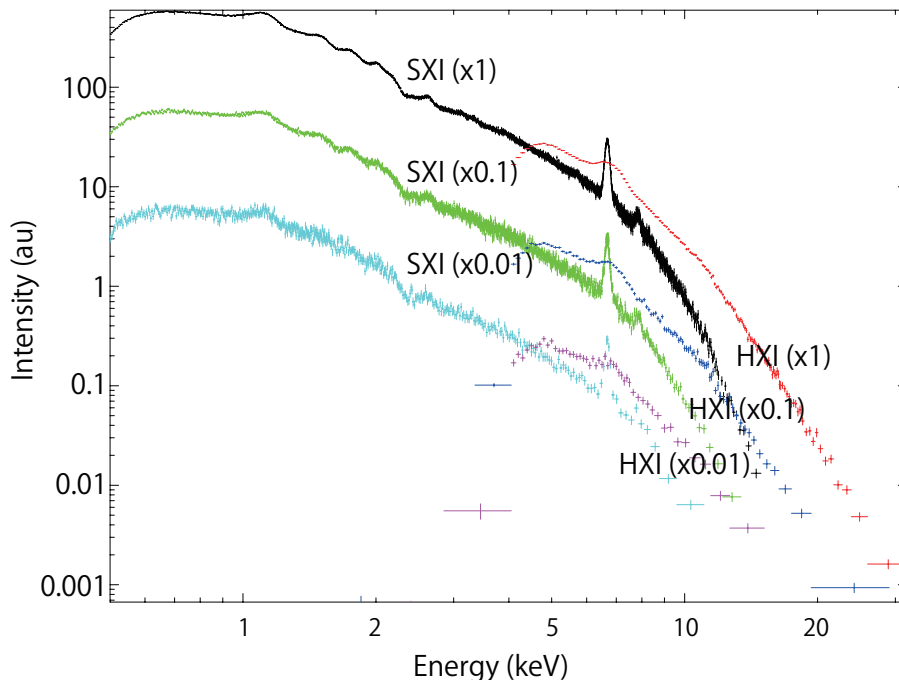


Figure 5: Simulated SXI+HXI spectra assuming an observed solar flare spectrum (Lin, 2011) and a flux of $\times 1$, $\times 0.1$, and $\times 0.01$ times of that observed in a large flare from UV Cet (Negoro et al., 2012) for 10 ks. Pile-up in the SXI detector is not considered.

Nearby (< 50 pc) bright sources that exhibit frequent flares are prospective candidates (e.g., VY Ari, UX Ari, V711 Tau, σ Gem, BO Mic, AR Lac, and II Peg). In figure 5, we show simulated SXI+HXI spectra assuming spectral distribution based on observations of a Solar flare, and with different fluxes. In the brightest case, the low energy cutoff in the power law at 20 keV is seen in the HXI spectrum. Figure 6 shows the simulated SXS spectra in the Fe K band for the same scenarios as in figure 5. A Doppler velocity of ~ 100 km s^{-1} is statistically distinguishable in the brightest two cases.

3.3.2 Planet-hosting Stars

HD 189733 is a primary target in this category, since this system showed an X-ray flare after secondary eclipse in two different occasions and thus has been suggested to possess a systematic SPI when the planet passes close to active regions on the host star (Pillitteri et al., 2011). The increased X-ray flux due to the flare mainly come in the Ne K band near 1 keV. Figure 7 shows SXS simulations of Ne lines during the flare from HD 189733 in three different cases, using parameters taken from a previously observed flare (Pillitteri et al., 2011). Even

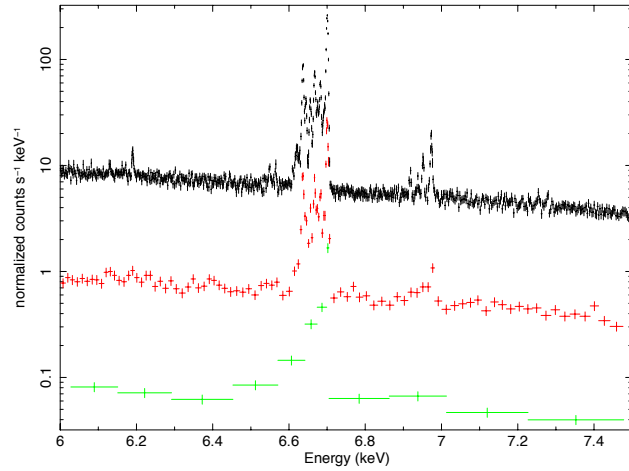


Figure 6: Simulated SXS spectra around Fe K emission assuming an observed solar flare spectrum (Lin, 2011) and a flux of $\times 1$, $\times 0.1$, and $\times 0.01$ times of that observed in a large flare from UV Cet (Negoro et al., 2012) for 10 ks.

with the large effective area of SXS, the statistical quality of the data is not sufficient to strongly constrain the plasma density. However, it still allows us to distinguish the low and high density limiting cases. It will also allow us to distinguish coronal emission from auroral charge-exchange emission, as has been observed in the polar regions of Jupiter (e.g., Hui et al., 2009).

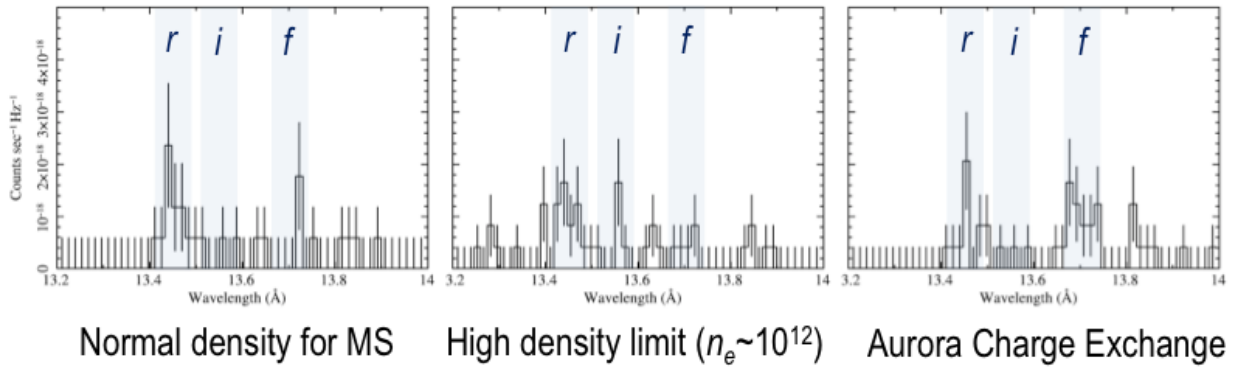


Figure 7: SXS simulations of a flare on HD 189733 in three different scenarios. Left: normal low density scenario for main-sequence stars. Center: high density scenario ($n_e \sim 10^{12}$). Right: auroral charge-exchange scenario.

4 Accretion Processes in Classical T Tauri Stars

4.1 Background and Previous Studies

The origin of the X-ray emission in young, accreting stars remains unclear. It has been known for decades that young stars display strong X-ray fluxes comparable to or higher than those in magnetically active stars (e.g., Feigelson & Montmerle 1999). High temperatures of several to several tens of millions of Kelvin and flaring both point to enhanced magnetic activity. No significant differences are observed between weakly accreting and strongly accreting T Tau stars, suggesting that accretion plays little if any role in the X-ray emission of young stars, despite the strong interplay expected between the accretion disk, infalling matter and the stellar magnetosphere.

This picture significantly changed with the advent of gratings onboard *Chandra* and *XMM-Newton*. Kastner et al. (2002) obtained the first X-ray grating spectrum of TW Hya, a moderately accreting classical T Tauri star (CTTS), and unexpectedly observed very low forbidden-to-intercombination lines ratios in the O VII and Ne IX He-like triplets, indicating high electron densities of the order of $10^{12} - 10^{13} \text{ cm}^{-3}$. The effect of UV photoexcitation on the observed line ratio was deemed negligible. In addition, the X-ray spectrum was consistent with a quasi-isothermal plasma of about 3 MK. Taken together, Kastner et al. (2002) concluded that the X-ray emission in TW Hya was due to accretion, a result further supported by observations with *XMM-Newton* (Stelzer & Schmitt, 2004) and with deeper *Chandra* observations (Raassen, 2009; Brickhouse et al., 2010).

The TW Hya results triggered a set of grating observations of CTTS. High electron densities were, indeed, found in the X-ray spectra of several CTTS (e.g., Schmitt et al., 2005; Günther et al., 2006; Robrade & Schmitt, 2007; Argiroffi et al., 2007, 2011, 2012; Huenemoerder et al., 2007). Despite the significant advancement made by grating spectroscopy, not many targets are bright enough for grating observations, and the achieved signal-to-noise ratios in typical exposures of the order of 100 ksec are very low (see Fig. 8). High efficiency non-dispersive spectroscopy capable of resolving He-like triplets would be highly beneficial to the understanding of the impact of accretion on the X-ray emission in young stars; of particular importance are the Ne IX, Mg XI, and Si XIII triplets, where critical electron densities range from about 10^{11} to 10^{13} cm^{-3} , probing the range of densities expected in accretion shocks.

Accreting CTTS further display a soft X-ray excess from plasma at low temperature (Telleschi et al., 2007; Robrade & Schmitt, 2007; Güdel & Telleschi, 2007). Such plasma, mostly detected in the O VII lines, is difficult to detect using CCD spectroscopy but can easily be revealed with high-resolution X-ray spectra when the absorbing column density is not too high. A soft X-ray excess can coexist with the hot plasma observed in the vast majority of young stars, which is due to scaled-up solar-like magnetic activity. The origin of such

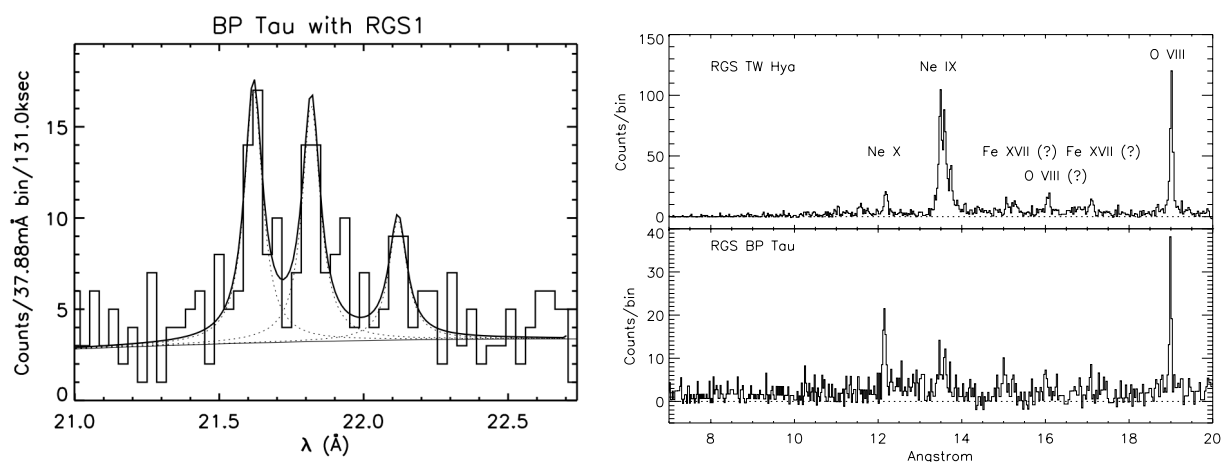


Figure 8: *XMM-Newton* RGS1 spectrum of BP Tau; the left panel shows the O VII triplet, and the right bottom panel shows the Ne IX triplet, with the Ne IX triplet of TW Hya shown in the right top panel for comparison (Schmitt et al., 2005). The exposure is 130 ks, showing the effective area limitations currently faced by grating spectroscopy.

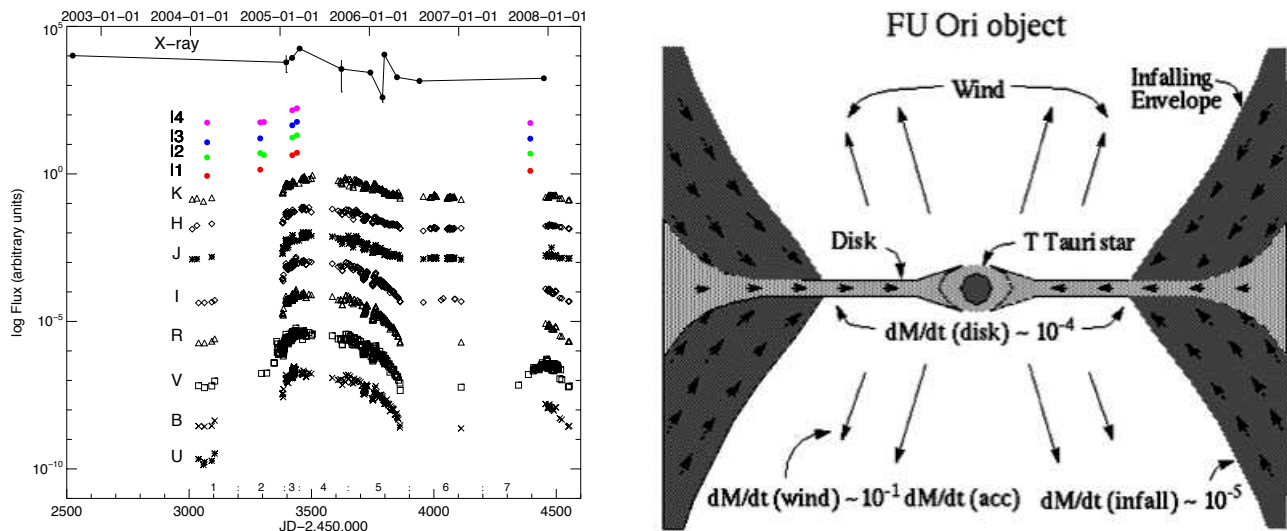


Figure 9: *Left:* X-ray, optical, and infrared light curves of V1118 Ori before, during, and after its outburst (Audard et al., 2010). *Right:* Schema of an FU Ori object, showing the strong interplay between the accretion disk and the stellar magnetosphere (Hartmann, 1997).

an excess is unclear, but it could be due in part to accretion onto the stellar photosphere. It is, therefore, crucial to understand how the X-ray emission in young stars, in particular those accreting matter actively, can be influenced by the accretion process.

While CTTS accrete matter in a somewhat "stable" fashion, though with some variability, a handful of accreting young stars display powerful eruptive events with flux increases in the optical regime of a few magnitudes. Two classes have emerged: FUors, which display outbursts of 4 magnitudes and more, last several decades, and therefore show a low recurrence rate; and EXors (named after the prototype EX Lup), which in contrast show somewhat smaller outbursts ($\Delta V = 2 - 3$ mag) on much shorter timescales, ranging from a few months up to a few years, and which may occur repeatedly (see review by Hartmann, 1997). Such outbursts are believed to originate during a rapid increase of the disk accretion rate from values of $10^{-7} M_{\odot} \text{ yr}^{-1}$ to $10^{-4} M_{\odot} \text{ yr}^{-1}$ over a short period of time. The limited number of eruptive young stars and the long recurrence time (especially for FUor-type objects) make it difficult to test models. It is therefore crucial to study the evolution of outbursts in as much detail as possible.

In the high-energy domain, eruptive stars have gained significant interest in the past few years. Initially triggered by the outburst of V1647 Ori, a young nearby low-mass star that erupted and illuminated McNeil's nebula, multi-wavelength observations monitored the outburst of other pre-main sequence accretion events and showed that X-ray variability closely tracks optical and infrared variability (Fig. 9; Kastner et al., 2004, 2006; Audard et al., 2005, 2010; Grosso et al., 2005, 2010; Lorenzetti et al., 2006; Teets et al., 2011, 2012; Hamaguchi et al., 2012). Although the exact behavior differs somewhat from star to star, the overall interpretation is that accretion significantly modified the magnetospheric configuration of the star-disk systems during and after the events (Audard et al., 2005, 2010; Kastner et al., 2006). Nevertheless, recent observations suggest that the star-disk magnetic field configurations may persist through multiple outbursts (Hamaguchi et al., 2012; Sicilia-Aguilar et al., 2012). In contrast, the X-ray spectra of FUors show hard emission (Skinner et al., 2006; Stelzer et al., 2009), with likely contamination by nearby nearby low-mass companions (Skinner et al., 2010). While they demonstrate the strong interplay between the accretion disk and the stellar magnetosphere, the X-ray spectra are strongly flux-limited and studies have focussed only on CCD spectroscopy. No measurements of He-like triplet diagnostics have yet been possible. The SXS will undoubtedly contribute in an unprecedented fashion in the understanding of accretion events in young stars.

4.2 Prospects & Strategy

ASTRO-H and the SXS in particular will determine electron densities in many young accreting stars thanks to

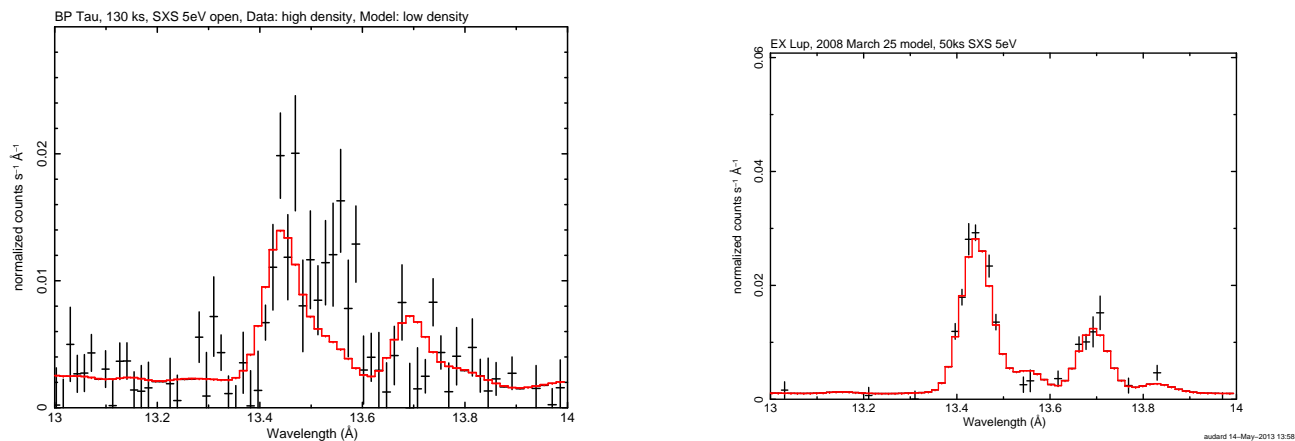


Figure 10: *Left:* Simulation of a 130 ksec SXS observation of BP Tau. Both high and low density cases are presented as data points and a model curve, respectively (Schmitt et al., 2005). *Right:* Simulation of a 50 ksec SXS observation of an outburst on EX Lup. The model used in the simulation is based on the data obtained on 25 Mar 2008 (Teets et al., 2012).

its sensitivity and its non-dispersive energy resolution.

Previous observations of young accreting stars with grating spectrometers onboard *XMM-Newton* and *Chandra* were rather rare (of the order of 15 targets), and many spectra had relatively poor signal-to-noise ratios. As an example, a 130 ks *XMM-Newton* observation of the nearby (140 pc) CTTS BP Tau barely detected the O VII triplet, although it managed to hint at an f/i ratio indicative of high densities (Fig. 8; Schmitt et al., 2005). The Ne IX triplet, although better detected, also showed limited signal, whereas the Mg XI or the Si XIII triplets were not detected. In contrast, *ASTRO-H* will be able to detect the Ne IX (Fig. 10, left) and Mg XI triplets, and likely the Si XIII triplet, with good signal-to-noise ratios and with much better spectral resolution above 1 keV than with grating spectroscopy¹. These lines will be crucial in probing the X-ray emission of young stars for which accretion plays a major role: they can probe densities of the order of 10^{11} to 10^{13} cm⁻³, a range of densities expected from X-ray emitting accretion shocks. Furthermore, they will be less sensitive to photoelectric absorption than the O VII triplet, which is often severely absorbed in young stars in star forming regions.

In the case of outbursting sources, *ASTRO-H* will provide the *first* ever measurement of densities in such young accreting stars. The observations, taken as soon as possible after the onset of the outburst will allow measurement of changes in electron density. In the current view, accreting material would partly fill in the stellar coronal loops and possibly change the magnetospheric configuration. *ASTRO-H* will allow to directly determine the amount of material accreted. Little or no change in electron densities would, on the other hand change dramatically the interpretation of the X-ray emission and suggest that accretion events trigger magnetic reconnection events in the young stellar corona.

ASTRO-H should ideally observe several “normal” accreting young stars to determine the electron densities from the Ne IX and Mg XI triplets in a moderately-sized but representative sample. A large sample would then provide a legacy survey of electron densities measured in young accreting stars.

The second approach, dedicated toward outbursting sources should focus on a ToO approach for EX Lup-type stars. The observation should be triggered by ground-based observations in the optical and near-infrared. The outburst should ideally be followed up by three to five *ASTRO-H* observations, and should include post-outburst observation to determine the conditions long after the accretion event. Short pre-outburst observations could be considered as well. In the case of FU Ori-type stars, an approach similar to “normal” CTTS is sufficient in view of the very long time scale of the outburst.

4.3 Targets & Feasibility

The science topic is oriented toward two sets of accreting young stars.

¹In terms of detecting weak lines, *ASTRO-H/SXS* has an advantage over *XMM-Newton/RGS* and *Chandra/LETGS* above 0.6 keV.

First, accreting young stars in nearby star forming regions should be observed. For example, the Taurus, Lupus, or Ophiuchus star forming regions include several tens of potential targets that could be observed. In view of the limited field-of-view of the SXS, the main instrument to address the science goals of this topic, pointed observations to select candidate members with promising X-ray spectra based on CCD spectroscopy should be chosen. In particular sources with soft X-ray components should be the prime targets.

Second, targets with known variable mass accretion rates displaying episodic accretion events should be observed, at least twice, once before an outburst, the second time in the early phase of the outburst, after some trigger obtained from optical/near-infrared ground-based observations. Although FU Ori-type targets would be ideal, they generally are either too embedded or too faint, notwithstanding the fact that a measurement in quiescence is unlikely in the time frame of the *ASTRO-H* mission. Instead, EX Lup-type objects, would be better suited. Several objects are possible, such as EX Lup, V1118 Ori, V1647 Ori. Due to the impossibility to predict which one of these targets would experience an accretion event after the launch of *ASTRO-H*, a TOO approach, with an observation timescale after trigger relatively flexible (several days to a few weeks are sufficient, the outbursts lasting several months to years), would be best. The second measurement could be derived either after the return to quiescence, or a survey of 2-3 potential targets in quiescence could be done in the early phases of *ASTRO-H*.

Two feasibility examples of measurements of Ne IX triplets are shown in Figure 10.

4.4 Beyond Feasibility

Observation of a strong X-ray outburst of a young star due to an accretion event is a definite bonus for this topic. In the present strategy, a TOO approach is foreseen, and such an outburst is therefore likely to be observed by *ASTRO-H*. The relatively frequent accretion activity observed in V1647 Ori, V1118 Ori, EX Lup, and other EX-Lup-type outbursting sources observed with *Chandra*, *XMM-Newton*, and *Suzaku* shows that such an event is likely to occur.

A second bonus would be an accretion event in a “normal” accreting CTTS, which would definitely show the link between the CTTS and the outbursting sources.

A final bonus would be the detection of a strong flare: young stars are also strongly magnetically active stars and should, therefore, display flares. This is described in detail in Topic 2.

5 Colliding Winds in Massive Stars

5.1 Background and Previous Studies

Massive binaries composed of a Wolf-Rayet (WR) star, a Luminous Blue Variable (LBV) star and an OB star often show higher temperature plasma compared to other early-type stars due to colliding winds. Ram-pressure balance between the two hypersonic winds determines the position of the colliding-wind region. The shocked plasma is expected to be heated to temperatures of 10^7 – 10^8 K. Colliding-wind binaries are ideal testing grounds for plasma-shock physics, mainly because plasma properties vary with binary separation in many cases.

Colliding wind binaries are important laboratories for investigating the physics of particle acceleration, since they provide access to higher mass, radiation and magnetic field energy densities than those in SNRs. High-spatial-resolution radio observations of synchrotron emission have revealed that the acceleration site is the region where the winds collide (e.g., Dougherty et al., 2005). In the X-ray band, the *Suzaku* HXD detected excess emission in the hard ($E > 10$ keV) band from η Car (LBV+WR: Sekiguchi et al., 2009) and WR 140 (WR+O: Sugawara et al., 2013). However, because of limited counting statistic in the HXD spectra, it is not possible to distinguish whether the hard excess is thermal or non-thermal.

Mass-loss rate, stellar wind acceleration, and rotation velocity are the most important and uncertain parameters in the evolution of a massive star. The mass-loss rate and the acceleration are usually measured using the radio and IR continuum flux together with modeling of spectral lines in the optical and IR bands. However, independent measurements of these parameters can be made in the X-ray band. The X-ray luminosity is highly dependent on the separation distance of the binary, the mass-loss rates, and wind velocities (Stevens et al. 1992; Usov 1992). If we know the orbital parameters of a binary, we can infer the mass-loss rate and wind-acceleration from the phase-dependent X-ray luminosity.

X-ray spectroscopy indicates that the profile of the neutral fluorescent iron line at 6.4 keV may be used to reveal the geometry of the wind-wind shock zone as well as wind and orbital parameters of colliding wind binaries. The neutral fluorescent iron line has been detected from two massive binaries (WR 6: Oskinova et al. 2012; η Car: Hamaguchi et al. 2007b; Fig 11). Unlike η Car, the spectrum of WR 6 shows a circumstellar absorption column density too small to explain the observed equivalent width of the neutral fluorescent line. The fluorescence must be emitted due to irradiation of the surface of the secondary by hard X-rays from the post-shock region, and the equivalent width therefore measures the solid angle subtended by the secondary surface from the point of view of the post-shock region.

5.2 Prospects & Strategy

We describe two possible observational techniques with *ASTRO-H* in the following section. First, we describe the use of broadband spectroscopy to constrain the origin of the hard excess. Second, we discuss the use of spectral lines to reveal the geometry of wind-wind shock zones and measure wind and orbital parameters of CWBs.

5.2.1 Broad-band spectroscopy

The *ASTRO-H* HXI will characterize the origin of the hard X-ray excess component, which may be related to γ -ray emission detected in massive star clusters (e.g., Cyg OB2, IC1805, NGC 6383). We would like to probe whether the hard excess is due to inverse Compton emission or thermal bremsstrahlung.

First we consider interactions between relativistic electrons and stellar UV photons (Bell, 1978). In the colliding wind region, first-order diffusive shock acceleration results in the production of a power-law spectrum of electrons with index 2 (White & Chen, 1995). The luminosity ratio of inverse Compton to synchrotron radiation can be written as $L_{\text{syn}}/L_{\text{IC}} = 840 B^2 r^2 / L_{\text{bol}}$, where the magnetic field B is expressed in G, r is the distance from the colliding-wind zone to the star in AU, and L_{bol} is the stellar luminosity in solar units.

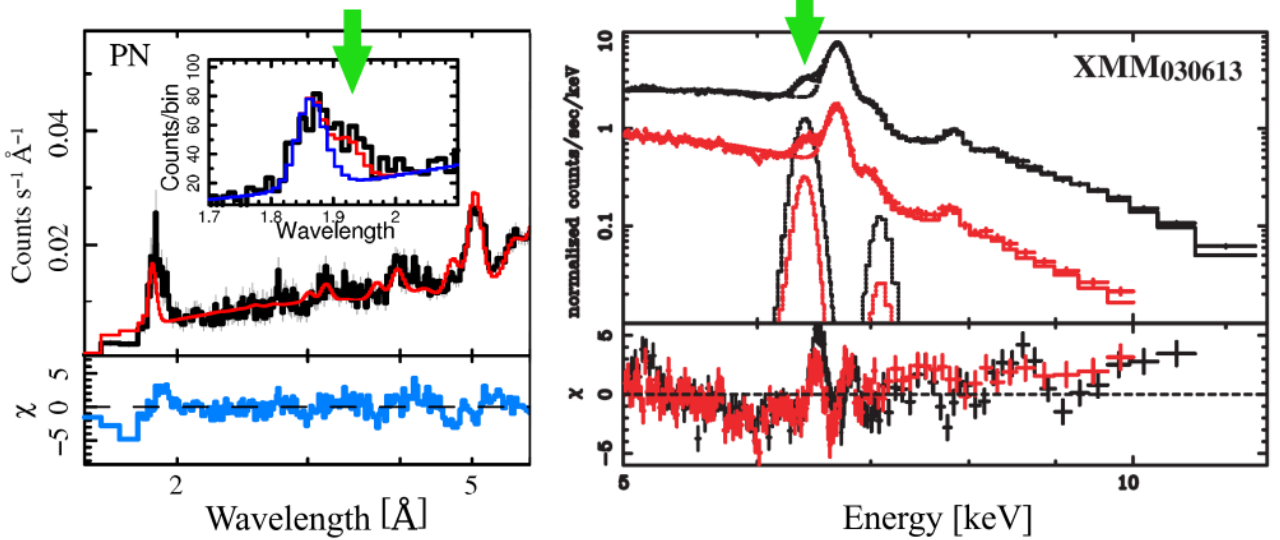


Figure 11: Fluorescent neutral iron lines (green arrow). *Left panel:* Spectra of WR 6 above 2 keV (from Fig.2 in Oskinova et al. 2012). Black shows the data of *XMM-Newton*/EPIC-pn. An insert to the top in the panel shows a broad spectral feature that is not reproduced by the thermal plasma model (blue). An additional fluorescent Fe line at 1.92 Å improves the fit (red). *Right panel:* Spectrum of η Car above 5 keV (from Fig.8 in Hamaguchi et al. 2007b). Black and red data points show *XMM-Newton*/EPIC-pn and *XMM-Newton*/EPIC-MOS1 spectra, respectively. The solid lines show the thermal plasma model together with additional fluorescent iron lines.

In the case of a strong adiabatic shock, the maximum electron temperature is given by

$$k_B T_e = \frac{3}{16} \mu_w m_p v^2 \sim 1.21 \text{keV} \frac{\mu_w}{0.62} \left(\frac{v}{1000 \text{ km s}^{-1}} \right)^2, \quad (2)$$

where μ_w is the mean atomic weight of the electron plus ion mixture, m_p is the proton mass, and v is the pre-shock wind velocity (cf. Antokhin et al. 2004). For example, if we suppose $v = 3000 \text{ km s}^{-1}$, the post-shock temperature is $k_B T_e \sim 18 \mu_w \text{ keV}$.

Using SXS, SXI and HXI on *ASTRO-H*, we will for the first time be able to differentiate between inverse Compton and thermal bremsstrahlung radiation.

5.2.2 Spectral lines

It is well known that the equivalent width of a neutral fluorescent iron line is proportional to the solid angle subtended by the reflector (e.g., Hayashi et al. 2011). For a colliding wind binary the fluorescent iron emission line at 6.4 keV therefore probes the site of the post-shock plasma, since the solid angle subtended by the secondary surface is related to its separation from the post-shock region; and by measuring the location of the post-shock plasma, we also obtain the wind momentum ratio of the binary.

Detection of a shoulder due to Compton backscattering of lines would further constrain the geometry (e.g., Watanabe et al. 2003; McNamara et al. 2008). The energy shift is related only to the backscatter angle (Fig 12).

5.3 Targets & Feasibility

η Car is one of the most suitable targets for *ASTRO-H*. It is a binary system (Damineli, 1996) containing a very massive LBV (“the primary”) and a hotter and less luminous evolved main-sequence companion (“the secondary”). η Car is one of the brightest colliding wind binaries in the X-ray band. Previous *Suzaku* and *XMM-Newton* observations show evidence for a hard excess and neutral Fe K fluorescent emission at 6.4 keV (Sekiguchi et al. 2009; Hamaguchi et al. 2007b).

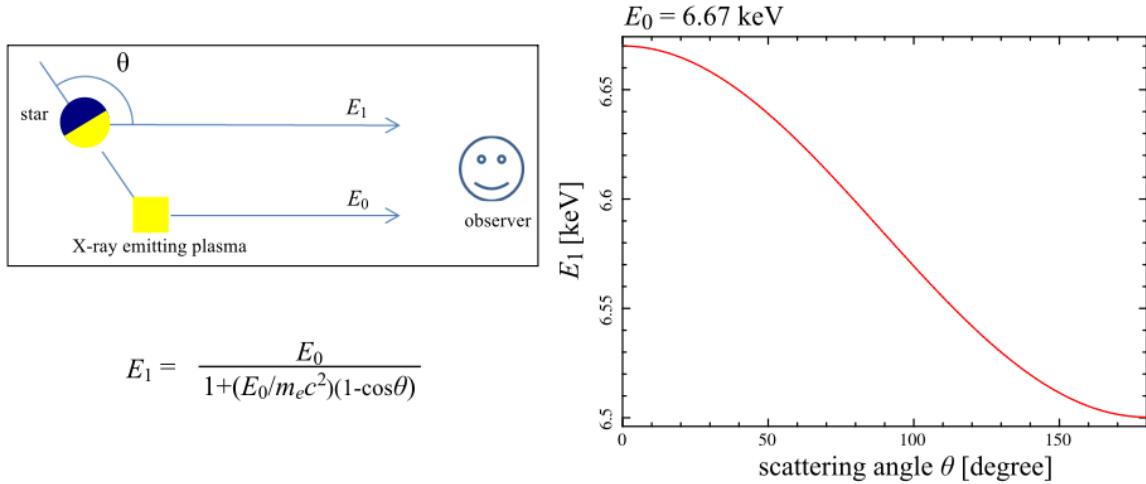


Figure 12: *Left panel:* A schematic view of Compton scattering. The equation shows the shift energy as a function of scattering angle. *Right panel:* The shift energy is shown as a function of scattering angle for rest energy $E_0=6.67$ keV.

We show simulated SXS and HXI spectra of η Car in a 50 ksec exposure in Figure 13. We simulated the spectra for two cases: inverse Compton (blue); and thermal bremsstrahlung radiation (red). These two cases can easily be distinguished by the HXI.

5.4 Beyond Feasibility

Luminous Blue Variables are a rare sub-class of massive star known to undergo extreme eruption events. The primary of η Car underwent two major eruptions in the 19th century. The most extreme LBV eruptions can result in mass loss of up to $10\text{--}40M_\odot$ or more (e.g., Smith & Owocki 2006). Kashi & Soker (2010) speculated that major eruptions are triggered by stellar companions and that in extreme cases a short duration event with a huge mass transfer rate can lead to a bright transient event on timescales of weeks to months (a “supernova impostor”). Observations of eccentric massive binaries at periastron passage could be an ideal opportunity to catch such an eruption. Observation of such an event could help constrain supernova theory.

In some CWBs, the wind momentum of the secondary may be insufficient to prevent the wind of the primary from colliding directly with the surface of the secondary, either for part or all of the binary orbit. This may occur at periastron in η Car, in which case it may be possible to measure the rotation velocity of the secondary. It might also be possible to make a similar measurement in systems where neutral Fe K fluorescence from the surface of the secondary is observed. Penny et al. (2004) analyzed the UV line profiles of 177 massive stars and suggested that the $v \sin i$ is at most 300 km s^{-1} , which is within the capabilities of the SXS. Stellar rotation speeds are critical ingredients in stellar evolution theory and in supernova explosions, with more extreme rotators considered to be likely candidates for Gamma-ray burst progenitors.

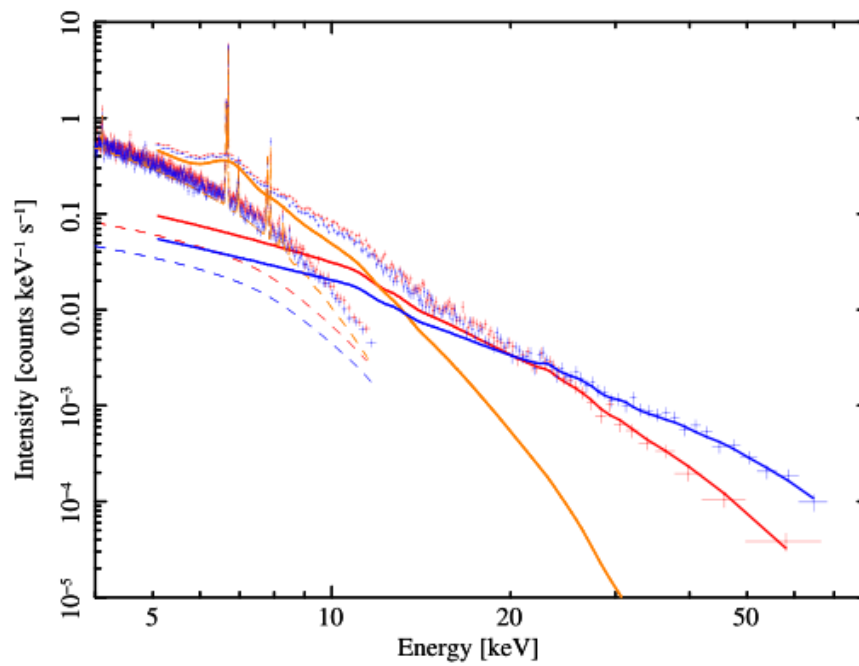


Figure 13: Simulated SXS+HXI spectra of eta Car in a 50 ksec exposure. The blue and red curves show the inverse Compton and very hot thermal bremsstrahlung radiation components, respectively, with solid and dashed curves showing this model for HXI and SXS, respectively. The orange curve shows the thermal radiation from the colliding wind shock.

6 Diffuse X-rays Associated with Star Forming Regions

6.1 Background and Previous Studies

Heavy elements such as carbon, oxygen, nitrogen, silicon and iron are produced inside massive stars through nuclear fusion. They are released to interstellar space by stellar winds and supernova explosions and enrich star forming clouds harboring young Suns. Supernova explosions eject matter in one event, while stellar winds from massive stars return more matter back to the interstellar medium gradually throughout the life of the star (e.g., Figure 6 of Meynet & Maeder, 2003). Both of these mechanisms contribute significantly to the chemical enrichment of the universe.

Transfer of heavy elements from massive stars to young stars can be witnessed in a massive star forming region (SFR) because massive stars evolve much more quickly than low mass stars. The diffuse X-ray plasmas which have recently been discovered in many massive star forming regions are suspected to originate from heated ejecta of massive stars, i.e., massive stellar winds and/or supernova remnants (RCW38: Wolk et al. 2002, M17: Townsley et al. 2003; Hyodo et al. 2008, Carinae Nebula: Hamaguchi et al. 2007a; Ezoe et al. 2008; Townsley et al. 2011, Orion Nebula: Güdel et al. 2008). Their physical parameters range from $kT \sim 0.1\text{--}0.8$ keV, $\log L_X$ up to 35 ergs s^{-1} , and size of $\sim 1\text{--}10^3$ pc. They tend to fill cavities of dense, cold molecular clouds where newly born young stars are embedded. Heavy elements in the plasmas may be absorbed into young solar systems through the cavity surfaces.

It is still controversial whether this X-ray emitting plasma originates primarily from supernovae or stellar winds. Supernova remnants (SNRs) such as Cas A, Kepler's remnant and the Cygnus loop have hot plasmas with $kT \approx 0.1\text{--}3$ keV. The strong spatial gradient in elemental abundances observed from the Carina nebula (Hamaguchi et al., 2007a; Townsley et al., 2011, see Figure 14, 15 *left panel*) is reminiscent of bullet-like ejecta in SNRs which are rich in silicon, sulfur, etc. However, unlike conventional SNRs, none of the diffuse X-ray plasmas in star forming regions has a spherical shape. Furthermore, compact relics expected from SNR explosions, black holes or neutron stars, have not yet been observed in these regions, with the exception of a middle aged neutron star found near the Carina Nebula (Hamaguchi et al., 2009; Pires et al., 2009), whose origin is under discussion. Even the Orion nebula shows diffuse X-ray emission, although it is quite young, has only late O type stars, and is not thought to harbor any SNR.

The Carina nebula also shows X-ray spectral features which are not apparently explained by emission from collisional equilibrium (CE) plasma. Townsley et al. (2011) found excesses in the best-fit spectra of many distinctive regions. The excesses can be reproduced with emission lines at $\sim 0.56, 0.76$ and 1.85 keV, where no strong emission lines from estimated plasma temperatures are present. The diffuse spectrum in the vicinity of η Car also shows a peculiar emission line at ~ 1.79 keV between the energies of fluorescent and Helium-like lines of silicon (Hamaguchi et al., in preparation, right panel of Figure 15). Some SNRs also show evidence for unidentified emission lines, which might be related to the unidentified emission lines from the Carina nebula. These lines may require strong Doppler shifts of nearby emission lines, or non-thermal processes such as charge exchange.

The dynamics of and physical process in these diffuse plasmas are crucial in understanding their origin and interaction with star forming clouds. We need to clearly resolve the emission lines around $0.5\text{--}1$ keV with better than CCD resolution. An *XMM-Newton* grating observation strongly constrained elemental abundances of the relatively concentrated ($\sim 1'$) diffuse emission around η Car (Leutenegger et al., 2003). The *ASTRO-H* SXS will expand this pioneering study to more extended regions with peculiar X-ray features and allow measurements of plasma dynamics and new physical processes in extreme conditions.

6.2 Prospects & Strategy

Diffuse X-ray plasmas in the SFRs, with typical temperatures of $\lesssim 0.8$ keV, emit K-shell emission lines of C, N, O, Ne, Mg and Si, and L-shell lines of Si, S, Fe and Ni. Among them, C, N, O, Si and Fe are the key products of nuclear fusion and therefore good probes to measure how stellar winds and/or supernova explosions inject energy and metals into the interstellar medium. These lines can be resolved clearly with the SXS and used for



Figure 14: X-ray emission from Carina (Townesley et al., 2011).

detailed diagnoses of plasma temperature, elemental abundance and ionization state.

Optical emission and absorption line studies suggest the presence of high velocity gas of a few 100 to several 1000 km s^{-1} along the lines of sights to a few massive stars, as well as warm gas around η Car (Walborn et al., 2002; Smith, 2008). This high velocity gas originates in flows from massive stars and/or from ancient supernova explosions and is likely associated with thermally emitting X-ray plasma. CCD resolution spectra have not detected any Doppler motions of the plasma above several 1000 km s^{-1} , but high resolution SXS spectra will be able to trace velocity shifts and broadening of these gases with much higher precision.

The SXS will clearly separate the heretofore unidentified emission lines observed in CCD spectra from known thermal emission lines, and hopefully detect more lines that are not expected from thermal plasma. Their identifications will be securely made with measurements of their line center energies at less than a few eV uncertainty. These lines will help to understand the physical processes and the origin of the diffuse X-ray emission.

The SXS should start approaching this science with a few selected regions in one or two SFRs with high X-ray surface brightness and which show interesting spectral features in earlier X-ray observations and/or other wavelengths. A survey can reveal spatial variation in plasma dynamics and elemental abundances in a SFR. Better yet, multiple surveys of SFRs may reveal the dependence of X-ray characteristics on the cloud mass and age. A suitable candidate, for example, would be a pair of regions in the Carina nebula, which show strong variations in the Fe and Si elemental abundances (Hamaguchi et al., 2007a; Ezoe et al., 2008; Townesley et al., 2011). The published *Chandra* survey of Carina (Townesley et al., 2011) can serve as a guide in selecting regions with interesting unidentified X-ray emission line features and which are dominated by diffuse emission with little contamination from point sources.

6.3 Targets & Feasibility

There are at least two distinct regions in the north and the south of the Carina nebula. Based on the *Chandra* studies of Broos et al. (2011) and Townesley et al. (2011), the best fields with high surface brightness and low contamination from point sources are: North: (R.A., Dec.) = (160.96070, -59.64274) (around the field “inside 51” in Townesley et al. 2011); South: (R.A., Dec.) = (161.04080, -59.85487) (around the field “inside 8” in Townesley et al. 2011). The combined point source flux between 0.5–2 keV in each of these fields is

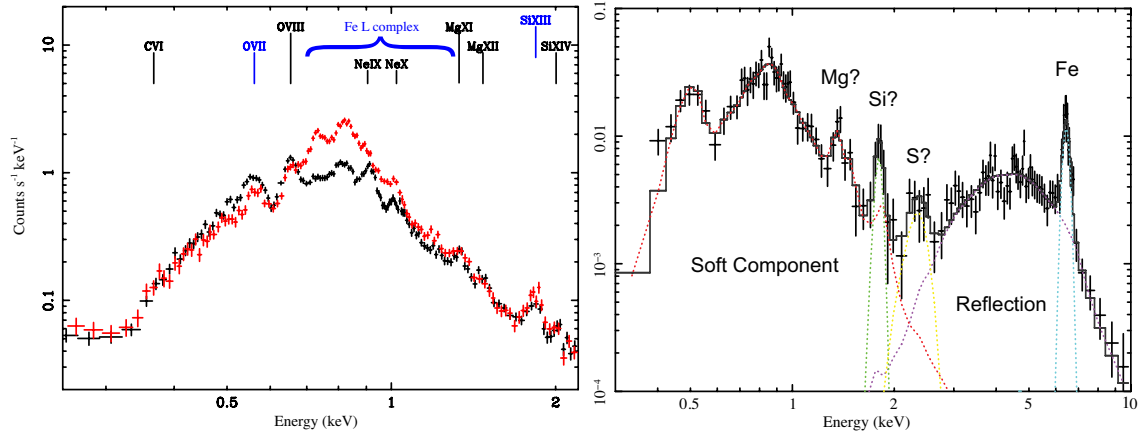


Figure 15: *Left:* Overlaid 0.3 – 2 keV spectra from the north (black) and south (red) regions of Hamaguchi et al. (2007a) in Carina. The north spectrum is normalized by 64% to adjust for the relative area compared to the south region at 2 keV. The labels show detected emission lines; lines labeled in blue exhibit distinct differences between the north and south spectra. *Right:* *Chandra* spectrum of the Homunculus nebula of η Car (Hamaguchi et al., in prep.). The spectrum shows peculiar strong emission lines around the silicon, sulfur and magnesium energies, which may originate from a non-thermal process such as charge exchange in collision of hot stellar winds with ambient cold gas.

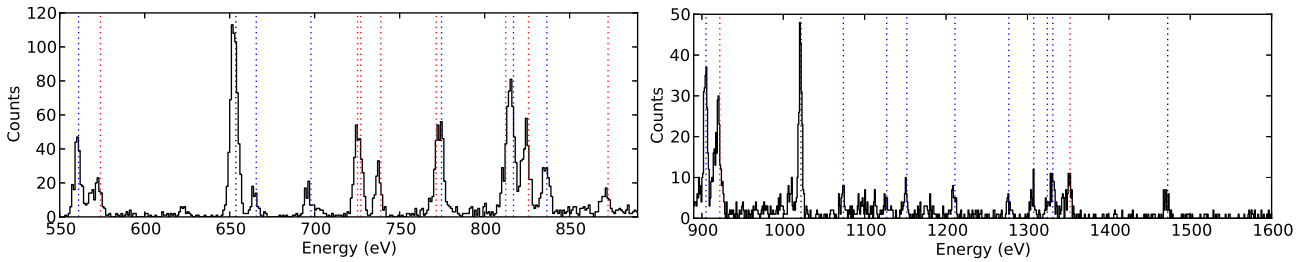


Figure 16: Simulated 30 ksec *ASTRO-H/SXS* X-ray spectrum of the central Carina nebula. The model assumes that half of the emission originates from hot, ionized plasma, and the other half from charge exchange of the same population of ions with cold gas. ISM absorption of $2 \times 10^{21} \text{ cm}^{-2}$ is included in the spectral model. The blue and red dotted lines indicate the positions of emission lines which are expected to originate primarily from charge exchange and thermal plasma, respectively; the black dotted lines indicate emission lines which are expected to have strong emission from both mechanisms.

$\sim 5 \times 10^{-14} \text{ ergs cm}^{-2} \text{ s}^{-1}$, which is about $\sim 5\%$ of the diffuse X-ray emission.

Other examples of SFR with diffuse X-ray emission are M17, RCW38, Rosette Nebula, and M42. They have significantly lower X-ray surface brightness than the Carina nebula, so that the SXS observations would require much longer exposure times ($\sim \text{Msec}$).

References

- Antokhin, I. I., Owocki, S. P., & Brown, J. C. 2004, *ApJ*, 611, 434
- Argiroffi, C., Maggio, A., & Peres, G. 2007, *A&A*, 465, L5
- Argiroffi, C., Flaccomio, E., Bouvier, J., et al. 2011, *A&A*, 530, A1
- Argiroffi, C., Maggio, A., Montmerle, T., et al. 2012, *ApJ*, 752, 100
- Asai, A., Hara, H., Watanabe, T., et al. 2008, *ApJ*, 685, 622
- Audard, M., Güdel, M., Skinner, S. L., et al. 2005, *ApJ*, 635, L81
- Audard, M., Stringfellow, G. S., Güdel, M., et al. 2010, *A&A*, 511, A63
- Bally J., Feigelson E., Reipurth B. 2003, *ApJ* 584, 843
- Bell, A. R. 1978, *MNRAS*, 182, 147
- Brickhouse, N. S., Cranmer, S. R., Dupree, A. K., Luna, G. J. M., & Wolk, S. 2010, *ApJ*, 710, 1835
- Broos, P. S., Townsley, L. K., Feigelson, E. D., Getman, K. V., Garmire, G. P., Preibisch, T., Smith, N., Babler, B. L., Hodgkin, S., Indebetouw, R., Irwin, M., King, R. R., Lewis, J., Majewski, S. R., McCaughrean, M. J., Meade, M. R., & Zinnecker, H. 2011, *ApJS* 194, 2
- Cuntz, M., Saar, S.H., & Musielak, Z.E. 2000, *ApJ*, 533, L151
- Damineli, A. 1996, *ApJL*, 460, L49
- Dougherty, S. M., Beasley, A. J., Claussen, M. J., Zauderer, B. A., & Bolingbroke, N. J. 2005, *ApJ*, 623, 447
- Ezoe, Y., Hamaguchi, K., Gruendl, R. A., Chu, Y.-H., Petre, R., & Corcoran, M. F. 2009, *PASJ*, 61, 123
- Favata, F., & Schmitt, J. H. M. M. 1999, *A&A*, 350, 900
- Favata F., Fridlund C. V. M., Micela G., Sciortino S., Kaas A. A. 2002, *A&A* 386, 204
- Feigelson E. D., Carkner L., & Wilking B. A. 1998, *ApJL* 494, L215
- Feigelson, E. D., & Montmerle, T. 1999, *ARA&A*, 37, 363
- Getman K. V., Feigelson E. D., Garmire G., Broos, P., & Wang, J. 2007, *ApJ* 654, 316
- Grosso, N., Hamaguchi, K., Kastner, J. H., Richmond, M. W., & Weintraub, D. A. 2010, *A&A*, 522, A56
- Grosso, N., Kastner, J. H., Ozawa, H., et al. 2005, *A&A*, 438, 159
- Güdel, M., & Telleschi, A. 2007, *A&A*, 474, L25
- Günther, H. M., Liefke, C., Schmitt, J. H. M. M., Robrade, J., & Ness, J.-U. 2006, *A&A*, 459, L29
- Güdel, M., Briggs, K. R., Montmerle, T., Audard, M., Rebull, L., & Skinner, S. L. 2008, *Science*, 319, 309
- Hamaguchi K., Corcoran M. F., Petre R., White N. E., Stelzer B., Nedachi K., Kobayashi N., & Tokunaga A. T. 2005, *ApJ* 623, 291
- Hamaguchi, K., Petre, R., Matsumoto, H., Tsujimoto, M., Holt, S. S., Ezoe, Y., Ozawa, H., Tsuboi, Y., Soong, Y., Kitamoto, S., Sekiguchi, A., & Kokubun, M. 2007a, *PASJ*, 59, 151
- Hamaguchi, K., Corcoran, M. F., Gull, T., et al. 2007b, *ApJ*, 663, 522
- Hamaguchi, K., Corcoran, M. F., Ezoe, Y., Townsley, L., Broos, P., Gruendl, R., Vaidya, K., White, S. M., Strohmayer, T., Petre, R., & Chu, Y. 2009, *ApJL*, 695, 4
- Hamaguchi, K., Grosso, N., Kastner, J. H., et al. 2012, *ApJ*, 754, 32
- Hartmann, L. 1997, *Herbig-Haro Flows and the Birth of Stars*, 182, 391
- Hayashi, T., Ishida, M., Terada, Y., Bamba, A., & Shionome, T. 2011, *PASJ*, 63, 739
- Huenemoerder, D. P., Kastner, J. H., Testa, P., Schulz, N. S., & Weintraub, D. A. 2007, *ApJ*, 671, 592
- Hayashi M., Shibata, K., Matsumoto, R. 1996, *ApJ* 468, 37
- Hui, Y., Schultz, D., Kharchenko, V., Stancil, P.C., Cravens, T.E., Lisse, C.M., & Dalgarno, A. 2009, *ApJ*, 702, L158
- Hyodo, Y., Tsujimoto, M., Hamaguchi, K., Koyama, K., Kitamoto, S., Maeda, Y., Tsuboi, Y., & Ezoe, Y. 2008, *PASJ*, 60, 85
- Imanishi K., Koyama K., Tsuboi Y. 2001, *ApJ* 557, 747
- Kamata Y., Koyama K., Tsuboi Y., Yamauchi S. 1997, *PASJ* 49, 461
- Kashi, A., & Soker, N. 2010, *ApJ*, 723, 602
- Kastner, J. H., Huenemoerder, D. P., Schulz, N. S., Canizares, C. R., & Weintraub, D. A. 2002, *ApJ*, 567, 434
- Kastner, J. H., Richmond, M., Grosso, N., et al. 2004, *Nature*, 430, 429
- Kastner, J. H., Richmond, M., Grosso, N., et al. 2006, *ApJ*, 648, L43
- Koyama K., Hamaguchi K., Ueno S., Kobayashi N., Feigelson E. D. 1996, *PASJ* 48, L87
- Koyama K., Maeda Y., Ozaki M., Ueno S., Kamata Y., Tawara Y., Skinner S., Yamauchi S. 1994, *PASJ* 46L, 125
- Lanza, A.F. 2009, *A&A*, 505, 339
- Leutenegger, M. A., Kahn, S. M., & Ramsay, G. 2003, *ApJ*, 585, 1015
- Lin, R. P. 2011, *Space Science Review*, 159, 421
- Lorenzetti, D., Giannini, T., Calzoletti, L., et al. 2006, *A&A*, 453, 579
- Makarov, V. V. 2003, *AJ*, 126, 1996

- McNamara, A. L., Kuncic, Z., Wu, K., Galloway, D. K., & Cullen, J. G. 2008, MNRAS, 383, 962
- Meynet, G., & Maeder, A. 2003, A&A, 404, 975
- Miller, B.P., Gallo, E., Wright, J.T., & Dupree, A.K. 2012, ApJ, 754, 137
- Montmerle T., Grosso N., Tsuboi Y., Koyama K. 2000, ApJ 532, 1097
- Negoro, H. et al. 2012. ATel #4671
- Oskinova, L. M., Gayley, K. G., Hamann, W.-R., et al. 2012, ApJL, 747, L25
- Osten, R. A., Drake, S., Tueller, J., et al. 2007, ApJ, 654, 1052
- Penny, L. R., Sprague, A. J., Seago, G., & Gies, D. R. 2004, ApJ, 617, 1316
- Pillitteri, I., Wolk, S.J., Cohen, O., Kashyap, V., Knutson, H., Lisse, C.M., & Henry, G.W. 2010, ApJ, 722, 1216
- Pillitteri, I., Günther, H.M., Wolk, S.J., Kashyap, V.L., & Cohen, O. 2011, ApJ, 741, L18
- Pires, A. M., Motch, C., Turolla, R., Treves, A., & Popov, S. B. 2009, A&A, 498, 233
- Pravdo S. H., Feigelson E. D., Garmire G., Maeda Y., Tsuboi Y., Bally J. 2001, Nature 413, 708
- Raassen, A. J. J. 2009, A&A, 505, 755
- Robrade, J., & Schmitt, J. H. M. M. 2007, A&A, 473, 229
- Rubenstein, E.P., & Schaefer, B.E. 2000, ApJ, 529, 1031
- Sakao, T., Kosugi, T., Masuda, S., Inda, M., Makishima, K., Canfield, R. C., Hudson, H. S., Metcalf, T. R., Wuelsel, J-P., Acton, L. W., Ogawara, Y. 1992, PASJ, 44, L83
- Schmitt, J. H. M. M., Robrade, J., Ness, J.-U., Favata, F., & Stelzer, B. 2005, A&A, 432, L35
- Sekiguchi, A., Tsujimoto, M., Kitamoto, S., et al. 2009, PASJ, 61, 629
- Sekimoto Y., Tatematsu K., Umemoto T., Koyama K., Tsuboi Y., Hirano N., Yamamoto S. 1997, ApJ 489, 63
- Sicilia-Aguilar, A., Kóspál, Á., Setiawan, J., et al. 2012, A&A, 544, A93
- Skinner, S. L., Briggs, K. R., Güdel, M. 2006, ApJ, 643, 995
- Skinner, S. L., Güdel, M., Briggs, K. R., & Lamzin, S. A. 2010, ApJ, 722, 1654
- Smith, N., & Owocki, S. P. 2006, ApJL, 645, L45
- Smith, N. 2008, Nature, 455, 201
- Stelzer, B., & Schmitt, J. H. M. M. 2004, A&A, 418, 687
- Stelzer, B., Hubrig, S., Orlando, S., et al. 2009, A&A, 499, 529
- Stevens, I. R., Blondin, J. M., & Pollock, A. M. T. 1992, ApJ, 386, 265
- Sugawara, Y., et al. 2013, submitted to PASJ
- Teets, W. K., Weintraub, D. A., Grosso, N., et al. 2011, ApJ, 741, 83
- Teets, W. K., Weintraub, D. A., Kastner, J. H., et al. 2012, ApJ, 760, 89
- Telleschi, A., Güdel, M., Briggs, K. R., et al. 2007, A&A, 468, 541
- Townsley, L. K., Broos, P. S., Chu, Y.-H., Gruendl, R. A., Oey, M. S., & Pittard, J. M. 2011, ApJS, 194, 16
- Townsley, L. K., Feigelson, E. D., Montmerle, T., Broos, P. S., Chu, Y.-H., & Garmire, G. P. 2003, ApJ, 593, 874
- Tsuboi Y., Imanishi K., Koyama K., Grosso N., Montmerle T. 2000, ApJ 532, 1089
- Tsujimoto, M., Koyama, K., Kobayashi, N., Saito, M., Tsuboi, Y., Chandler, C. J. 2004, PASJ, 56, 341
- Usov, V. V. 1992, ApJ, 389, 635
- Yang, X. et al. 2009, RA&A, 9, XX
- Walborn, N. R., Danks, A. C., Vieira, G., & Landsman, W. B. 2002, ApJ, 140, 407
- Watanabe, S., Sako, M., Ishida, M., et al. 2003, ApJL, 597, L37
- White, R. L., & Chen, W. 1995, Wolf-Rayet Stars: Binaries; Colliding Winds; Evolution, 163, 438
- Wolk, S. J., Bourke, T. L., Smith, R. K., Spitzbart, B., & Alves, J. 2002, ApJL, 580, 161